RESEARCH PAPER

CrossMark

A new constitution diagram for dissimilar metal welds of high-manganese steels

Benjamin Wittig [1] · Manuela Zinke [1] · Sven Jüttner [1] · Daniel Keil [2]

Abstract

When dissimilar metal welding of high-manganese (Fe-Mn) steels with low-alloyed steels, martensite may form in the weld metal. Current constitution diagrams for weld metal microstructure prediction cannot be used for Fe-Mn steels since the influence of the high manganese content in those steels is not sufficiently considered in the Ni equivalent. This paper concentrates on the development of a new constitution diagram for reliable weld metal microstructure prediction when dissimilar metal welding of Fe-Mn steels with low-alloyed ferritic and martensitic steel grades. For developing the constitution diagram a specially designed arc melting technique was used to experimentally simulate dissimilar weld metals in different dilutions and compositions. The resulting samples were evaluated regarding the type and quantity of the microstructural phases by means of hardness and ferrite number measurements as well as light-optical microscopy. Using this dataset it was possible to determine functional correlations between the chemical composition and the weld metal microstructures. By means of statistical analysis, a new constitution diagram was developed. Actual GMAW welds of different material combinations were performed to validate the applicability of the diagram. The new constitution diagram has a very high prediction accuracy and also distinguishes between the different types of martensite (ε and α').

Keywords (IIW Thesaurus) Dissimilar materials · Austenitic manganese steels · Schaeffler diagram · Phase diagram · Dilution · Martensite · Weld metal · Microstructure

1 Introduction

In recent years, particular importance has been attached to austenitic Fe-Mn steels for applications in automotive vehicle structures. These steels achieve excellent mechanical properties in terms of high strength and plasticity due to the TWIP (twinning-induced plasticity) effect. [1, 2] Particular challenges in fusion welding of those new steel grades result from their integration in existing structures of established high strength auto body steels, such as ferritic or martensitic steels. Previous studies showed the presence of martensitic constituents in the

✉ Benjamin Wittig
benjamin.wittig@ovgu.de

1   Institute of Materials and Joining Technology, Otto von Guericke University, Magdeburg, Germany

2   Group Research, Volkswagen AG, Wolfsburg, Germany

dissimilar weld metal depending on dilution, welding process, and cooling conditions as well as the used filler metal for those dissimilar metal welds (see Fig. 1). This can lead to brittle component failure under dynamic or multiaxial loads. [3, 4]

Historically, industrial users utilized constitution diagrams for determining the weld metal microstructure. However, current available and also scientifically recognized diagrams, such as the Schaeffler diagram or the WRC-1992 diagram cannot be used for the novel Fe-Mn steels. The effect of their very high manganese content of 15 to 25 wt.-% is not sufficiently considered in the nickel equivalent.

Klueh et al. [5] and Lee et al. [6] developed modifications of the Schaeffler diagram particularly for high-manganese steels (see Fig. 2). Klueh et al. [5] realigned the boundary lines in the Schaeffler diagram. This modified Schaeffler diagram was used as basis in Lee's investigations [6] to adapt the equivalents. However, the applicability of these diagrams for the prediction of weld metal microstructures should be questioned. The test alloys used to create the diagrams were not produced under actual welding conditions, but as rolled products with a final annealing process for several hours
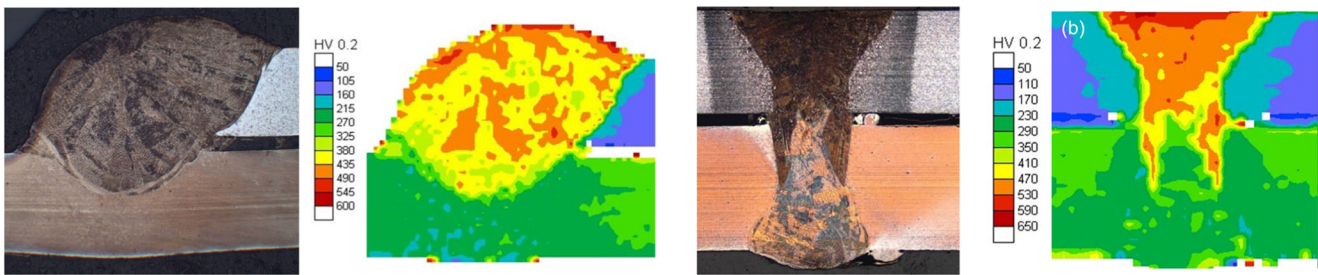
Fig. 1 Hardening structure in the weld metal of a dissimilar GMAW and laser beam joint consisting of an austenitic Fe-Mn steel (lower sheet) and the ferritic steel HX340LAD (upper sheet) [3]

between 1000 and 1150 °C and subsequent cooling under helium atmosphere or water quenching. The maximum temperature as well as the heating-up, holding, and cooling conditions have a significant influence on the transformation and precipitation conditions, so that the microstructures of the wrought alloys and weld metals can differ significantly [7].

Since there is no constitution diagram for reliable microstructure prediction for dissimilar metal welds of high-manganese steels, the objective of this study was to develop a new constitution diagram for dissimilar metal welding of austenitic Fe-Mn steels in combination with low-alloyed ferritic or martensitic steels. The focus of the investigations was not only on the development of functional relationships between the alloying elements and the microstructure formation but also on the correlation between the weld metal microstructure and the resulting properties, e.g., the weld metal hardness.

2 Experimental

2.1 Test materials

Materials for this study included three different austenitic Fe-Mn steels with varying alloying content, along with a ferritic low-alloyed steel HC340LA (EN 10268 [8]) and a press-

hardenable boron-manganese steel 22MnB5 (EN 10083-3 [9]), which has a ferritic-pearlitic microstructure as delivered. The base metals are received in as-rolled condition with a sheet thickness ranging from 1.5–3.0 mm. In addition, three different high-manganese welding consumables are used besides the commercial available Cr-Ni filler metal ISO 14343-A - G 18 8 Mn (FM-III) and the low-alloyed filler metal ISO 14341-A-G 3Si1 (FM-V). Table 1 shows the chemical composition of the test materials.

2.2 Experimental weld metal simulation

Most of the established constitution diagrams were determined on the basis of the evaluation of numerous actual weld metals, which were iteratively produced in various combinations of base and filler metals and different dilutions. An alternative to this very laborious procedure is a simple arc melting technique, also known as button melting technique [10–12]. This procedure has already been successfully applied by Balmforth and Lippold to create a constitution diagram for dissimilar metal welds of ferritic and martensitic steels [10, 13].

Based on the principle of the button melting technique an arc melting technique was set up and optimized that enables an experimental simulation of dissimilar weld metals, which
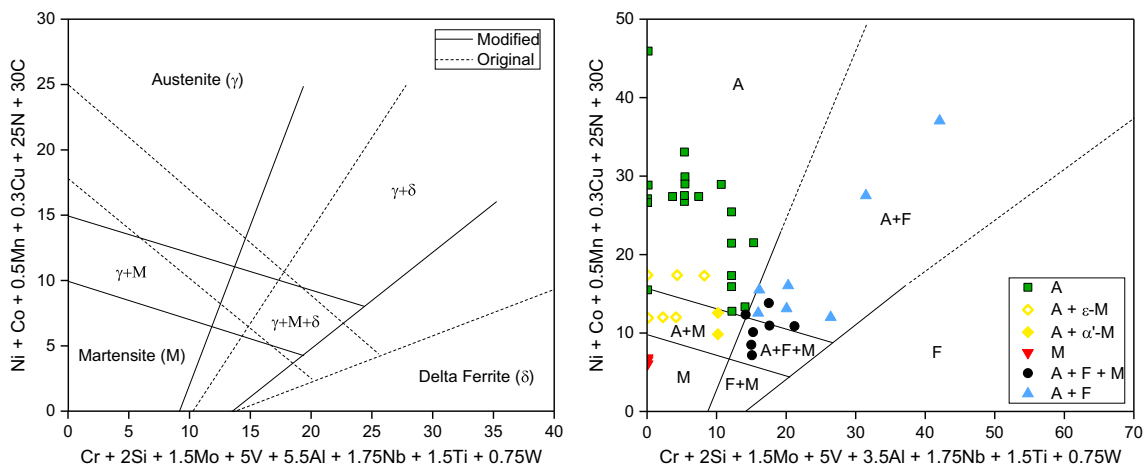

Fig. 2 Modified Schaeffler diagram according to Klueh et al. [5] (left), and modification of the equivalents according to Lee et al. [6] (right)

Table 1 Chemical composition (wt.-%) of the test materials

Test materials	C	Mn	Al	Si	Cr	Ni	P	S	Fe and other
Austenitic Fe-Mn steels									
Fe-Mn-I	0.37	19.1	1.21	0.54	2.10	0.30	0.020	<0.001	Bal.
Fe-Mn-II	0.65	15.3	2.30	2.23	0.08	0.10	0.006	0.0002	Bal.
Fe-Mn-III	0.30	15.9	0.003	0.16	14.7	0.41	0.025	0.003	Bal.
Ferritic/martensitic steels									
HC340LA	0.09	1.0	0.03	0.29	0.02	0.01	0.017	0.007	Bal.
22MnB5	0.23	1.2	0.04	0.24	0.11	0.01	0.017	0.005	Bal.
Filler metal									
FM-I	0.60	17.4	–	0.33	–	–	0.002	0.009	Bal.
FM-II	0.64	14.5	0.02	0.74	4.0	0.21	0.002	<0.031	Bal.
FM-III	0.08	7.0	–	0.80	19.0	9.0	0.002	0.009	Bal.
FM-IV	0.15	17.6	0.04	0.006	0.02	–	0.002	0.003	Bal.
FM-V	0.07	1.5	–	0.86	0.03	0.01	0.01	0.016	Bal.

was already shown in detail in previous articles [14, 15]. Samples of different material combinations are melted in a range of dilutions using a GTA process in a water-cooled copper crucible under argon atmosphere (see Fig. 3). Homogeneous mixing in the sample is obtained by a rotary movement of the GTA electrode and multiple remelts. As a result of optimization measures (e.g., crucible shape) it is possible to produce dissimilar weld metals of any material combination in defined dilutions under GMAW adequate cooling conditions (cooling time $t_{8/5}$ = 11–15 s). Thus time-consuming and cost-intensive processes of iterative production of actual welds can be avoided.

A significant factor for the resulting microstructure constitution in dissimilar weld metals is the dilution. According to Herold [16], it is defined as the unavoidable pick up of base metal, filler metal or metal from already welded beads or layers in the welding zone. The degree of dilution Φ specifies the area proportions or mass proportions of the melted joining partners in relation to the total weld metal. In the context of the experimental weld metal simulation, the degree of dilution is to be understood as the mass ratio of the joining partners. The degree of dilution is designated hereinafter as Φ_j, with j = A (austenitic Fe-Mn steel), F (ferritic steel), or M (martensitic steel).

The test materials were combined in a variety of different combinations and dilutions to produce a wide range of different weld metal microstructures and chemical compositions.

This should ensure both a precise determination of the boundary lines between the resulting types of microstructures and a reliable development of functional relationships between chemical composition and type of microstructure.

2.3 Weld metal characterization

The dissimilar weld metals were characterized by hardness (HV10) and ferrite number (FN) measurements as well as light-optical microscopy (LOM) performed on cross-sections through the center of the samples. The correlation of hardness and FN provided an initial evidence of the forming microstructural phases in the weld metal as shown in a previous paper [14]. In dissimilar weld metals of Fe-Mn steels, the two types of martensite ε and α' can form. However, only α'-martensite has ferromagnetic characteristics in contrast to the paramagnetic ε-martensite [17, 18]. Therefore, a simultaneous increase in hardness and FN is only to be expected in the case of α'-martensite formation. The correlation of hardness and FN can also be used to distinguish between martensite and ferrite. For example, an increase in FN with a simultaneous decrease in hardness indicates ferrite formation [14]. The FN was measured using a Fischer-Feritscope® MP3C. Based on a magnetic induction, the device records all ferromagnetic constituents. LOM provided the final information about the present microstructural constituents by revealing
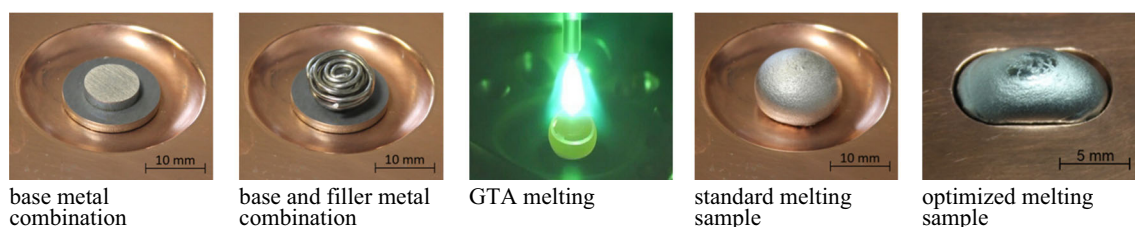

base metal combination   base and filler metal combination   GTA melting   standard melting sample   optimized melting sample

Fig. 3 Illustration of the process from the base material to the melting sample

the morphological appearance of the phases. For this purpose, a number of different etchants were used including mainly Klemm I, LePera and Beraha. Most of the alloys responded well to Klemm I, but at higher Cr contents LePera and Beraha delivered better contrasts between the phases.

2.4 Statistical data analysis

The alloying elements most commonly used in steels can be subdivided into two groups. These are the austenite formers (e.g., Ni, C, Mn) that promote the formation of the non-magnetic, face-centered-cubic austenite, and the ferrite formers (e.g., Cr, Mo, Si, Ti), which promote the formation of the magnetic, body-centered-cubic ferrite. To determine which elements and their coefficients should be used in the new equivalency relationships for the prediction of weld metal microstructure, statistical classification methods were used. The type of microstructure (austenite, austenite + martensite, etc.) was defined as the dependent variable, while the elements affecting the phase stability were defined as the independent (explanatory) variables. The objective of the classification analysis was to determine simple prediction rules that allow the user to estimate the resulting microstructure at a glance. The new diagram should linearly combine austenite and ferrite formers in separate equivalent formulas as established in previous constitution diagrams. These linear combinations should be recorded at the horizontal and vertical axes in a two-dimensional system. For the classification based on the available data an approach via a canonical discriminant analysis was used, which is also applicable when the data are not normally distributed. [19] The discriminant analysis was performed using SPSS Statistics software. This process produces a linear combination of the form:

$$Y = b_1 X_1 + b_2 X_2 + \ldots + b_j X_j \tag{1}$$

In this case, Y is the discriminant variable and b_j are the coefficients for the alloying elements X_j. The elements initially included in the discriminant analysis were C, Mn, Ni, Cr, Al, Si, Mo, Co, Ti, N, and Cu. Starting from a canonical discriminant analysis including all elements, all subsets of variables were tested, which produced a variety of linear combinations. Various potential discriminant functions including different combinations of elements with different coefficients were developed. These discriminant functions were examined regarding the success rate of accurate classification of the data by cross-validation. Moreover, it was checked whether the coefficients have the expected signs to provide meaningful interpretations. The optimum solution was chosen in terms of prediction accuracy and metallurgical plausibility.

3 Results and discussion

3.1 Effect of dilution on weld metal properties

The results of the FN measurements show an increase of the FN with increasing dilution of ferritic or martensitic joining partner (cf. Table 1) as expected. Fig. 4 shows an example of this phenomenon using a material combination of Fe-Mn-II and 22MnB5. The threshold between paramagnetic (FN = 0) and ferromagnetic (FN > 0) response of the dissimilar weld metals varies slightly depending on the material combination and dilution. In the example of Fig. 4 this threshold is at a dilution of $\Phi_M = 30\%$ (FN = 0.2). Also in the overall view for all material combinations, this threshold is reached at a dilution Φ_F or Φ_M of approx. 30%. The ferromagnetic response is a first indication for the formation of α'-martensite in the weld metal. The trend of the hardness is very similar to the FN. In the example of Fig. 4 the hardness is comparatively low (~ 200 HV10) up to a dilution of $\Phi_M = 40\%$, but then increases significantly, which also indicates a martensite formation. When looking at the correlation between hardness and dilution for all material combinations (see Fig. 7 later in this paper), the hardness is less than 300 HV10 if the dilution Φ_F or Φ_M is below 30–40% and then increases rapidly. However, while the hardness decreases after passing through a maximum at a dilution Φ_F or Φ_M of approx. 60–80%, the FN increases continuously until reaching its maximum at a dilution of 100%. This characteristic suggests a gradual formation of ferrite at higher dilutions.

As a result of the metallographic characterizations by LOM, the following types and combinations of microstructures are distinguished that are present in the weld metal depending on material combination and dilution (see Fig. 5):

- **A** = austenite
- **A+F** = austenite + ferrite
- **A+M(ε)** = austenite + ε-martensite
- **A+M(ε) + F** = austenite + ε-martensite + ferrite
- **A+M(α')** = austenite + α'-martensite
- **M(α')** = α'-martensite
- **M(α')+F** = α'-martensite + ferrite
- **F** = ferrite

This confirms the assumptions made on the basis of FN and hardness. Depending on the material combination, martensite forms for the first time in samples with a dilution Φ_F or Φ_M of approx. 10–30% (see Fig. 7). At low dilutions of ferritic or martensitic steel and high amounts of Fe-Mn steel, a multiphase microstructure consisting of A+M(ε) is present, whereas α'-martensite is forming at higher dilutions Φ_F or Φ_M. The FN was used here complementary to distinguish between ε- and α'-martensite taking advantage of their ferromagnetic
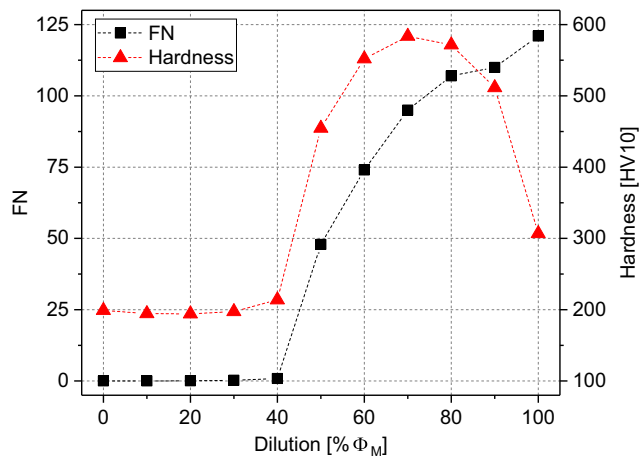
Fig. 4 Effect of dilution on hardness and FN using the example of the dissimilar weld metal of Fe-Mn-II and 22MnB5

characteristics. The paramagnetic ε-martensite is optically characterized by a structure of thin, flatly bounded plates, which partly have a ribbon-like shape (see Fig. 5 b). Schumann [17, 18, 20] already described the possibility of the formation of ε-martensite in Fe-Mn alloys with high Mn content (> 10% Mn) and low stacking fault energy. The α'-martensite that is formed with increasing dilution Φ_F or Φ_M occurs in the dissimilar weld metals in the morphological appearance of both the plate and the lath martensite. The needle-shaped plate martensite is found together with fractions of residual austenite (see Fig. 5 e), whereas the lath martensite shows a massive appearance without residual austenite (see Fig. 5 f). Furthermore, mixed forms of ε- and α'-martensite can also be assumed, but these cannot be clearly separated metallographically. Additional XRD analyses were used to prove the simultaneous presence of ε- and α'-martensite [21], but the analysis of every single sample using XRD would have been too expensive due to the high amount of

samples. For this reason, the double formation of martensite was not considered as a separate microstructure constitution.

Studies regarding the hardness of weld metal depending on the type and fraction of martensite show that samples having a high amount of ε-martensite are relatively soft (< 250 HV10), while samples having the same amount of α'-martensite instead of ε-martensite are more than twice as hard to some extent (see Fig. 6). In conclusion, a high martensite fraction without distinction between ε- and α'-martensite is not an evidence for a hard weld metal structure. Therefore, it is important for the subsequent analysis and correlations to differentiate between ε- and α'-martensite.

As can be seen from the correlation of microstructure and hardness as a function of dilution Φ_F or Φ_M (see Fig. 7), the formation ε-martensite does not affect the hardness significantly. As already mentioned above, the hardness starts to increase significantly at a dilution Φ_F or Φ_M of about 40%. The correlation with the results obtained by LOM shows that this is directly related to the formation of α'-martensite. The highest hardness values are determined in the A+M(α') and M(α') microstructures at dilutions Φ_F or Φ_M of approx. 60–80%.

3.2 Statistical data evaluation and development of the new constitution diagram

The arc melting technique was used to produce a large number of dissimilar weld metals over a wide range of different compositions. A total of 132 differently alloyed weld metals were produced and characterized with regard to hardness, FN and microstructure. The classification of the samples using the Schaeffler diagram shows a poor correlation to the actual weld metal microstructures, as already expected (see Fig. 8 left). Only 64% of the data are classified correctly. The Schaeffler diagram predicts martensite in compositions that are
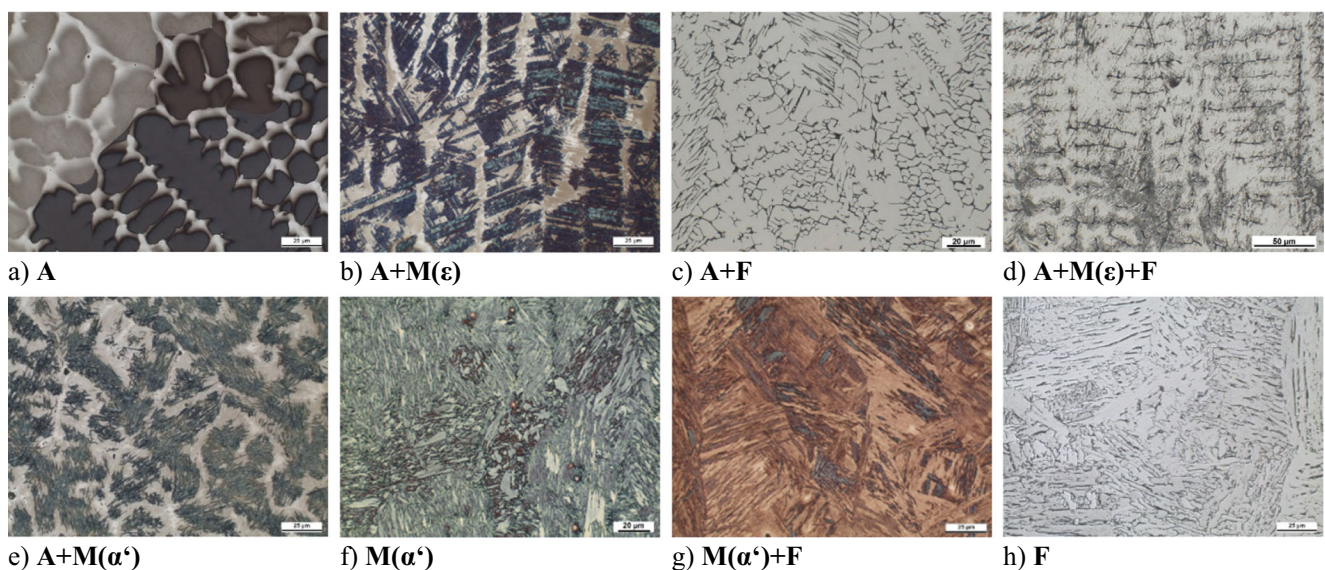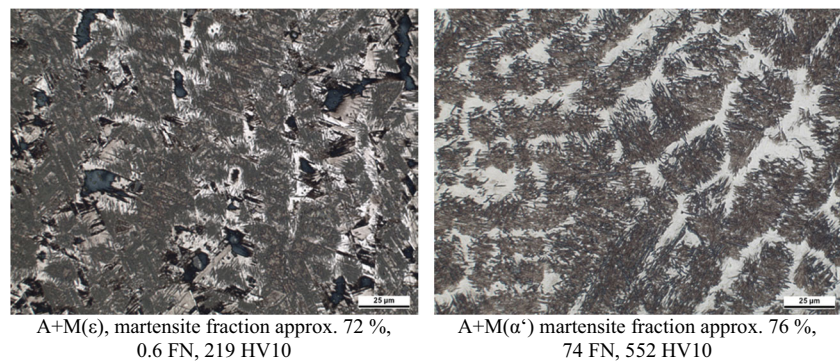

a) **A**   b) **A+M(ε)**   c) **A+F**   d) **A+M(ε)+F**

e) **A+M(α')**   f) **M(α')**   g) **M(α')+F**   h) **F**

Fig. 5 Representative weld metal microstructures of different material combinations and dilution. Etchings: Klemm I (a, b, e–g), Beraha (c, d, h). M: × 500

Fig. 6 Comparison of weld metal microstructures with approximately equal martensite contents but different types of martensite. Etching: Klemm I. M: × 500

A+M(ε), martensite fraction approx. 72 %, 0.6 FN, 219 HV10

A+M(α') martensite fraction approx. 76 %, 74 FN, 552 HV10

martensite-free and a mere shift of the microstructure boundaries is not appropriate because of the high overlap of different types of microstructures when using the Schaeffler equivalent formulas. Moreover, the Schaeffler diagram does not differentiate between ε- and α'-martensite.

The new equivalent formulas were developed using canonical discriminant analysis. This led to a complex mathematical correlation for classifying the data. To obtain a two-dimensional illustration, the number of discriminant functions had to be reduced. In the present situation, only the first discriminant function was used to constitute the equivalent formulas. Thus, the alloying elements were combined linearly with the coefficients of the first discriminant function as follows:

$$Y = (10.563 \times C + 0.523 \times Mn + 0.682 \times Ni)$$
$$+ (0.278 \times Cr + 0.756 \times Al{-}0.590 \times Si) \quad (2)$$

The coefficients were multiplied by a scaling factor and practically rounded. Then the discriminant function was divided into two separate equivalents. In accordance with the established constitution diagrams, the equivalent with the austenite formers was placed on the vertical axis and that with the ferrite formers on the horizontal axis (see Fig. 8 right).
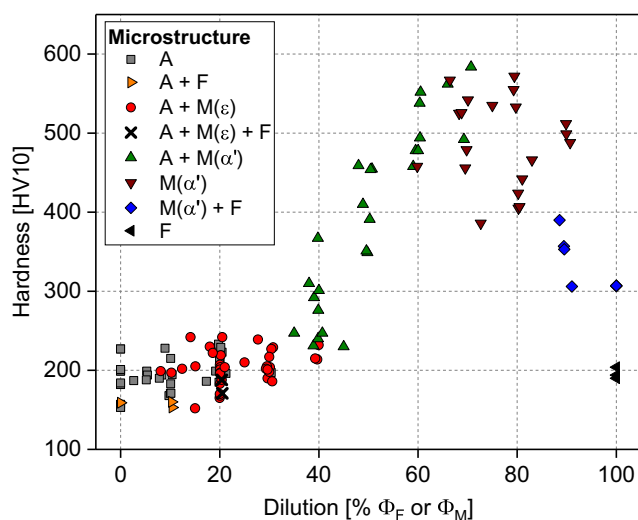

Fig. 7 Effect of dilution on weld metal microstructure and hardness

Furthermore, a correction factor of 2.5 was added in the equivalent of the horizontal axis so that all points are located in the first quadrant. The sectioning between the microstructure regions is arranged by straight lines.

The newly developed constitution diagram, the COHMS diagram (short for **C**onstitution **o**f **H**igh **M**anganese **S**teel Welds), classifies 93% of the weld metal microstructure correctly. The other 7% are close to the boundary lines. Besides the different coefficients and the additional distinction between ε- and α'-martensite, a significant difference to the Schaeffler diagram (and also to other diagrams) is that silicon is assigned with a negative factor. In principle, silicon is one of the ferrite formers, so a positive coefficient would have to be assumed. However, in Fe-Mn steels, silicon reduces the amount of the face-centered-cubic austenite phase and promotes the formation of martensite [3]. Studies by Zhao [22] on the influence of silicon on martensite transformation show that the martensite starting temperature increases significantly with increasing Si content. According to this, it can be supposed that a martensite formation in dissimilar weld metals of Fe-Mn steels is also promoted by silicon, which is indicated by the negative sign.

The statistical software could not estimate a clear influence for nitrogen. This is probably due to the fact that the Fe-Mn steels have only very low nitrogen contents. Since the influence could not be calculated, it cannot be taken into account in the equivalent formulas. However, the high classification accuracy indicates that there should not be any negative implications.

3.3 Validation of the COHMS diagram

The applicability of the constitution diagram for microstructure prediction in dissimilar GMAW welds was evaluated by GMAW-CMT lap welds. For this purpose, mainly dissimilar joints and also partly similar joints were produced for selected material combinations with different degrees of dilution. To achieve different dilution ratios, the variation of torch offset and wire feed speed (≙ welding current) was mainly used. The heat input per unit length varied between 2.4–4.4 kJ/cm,
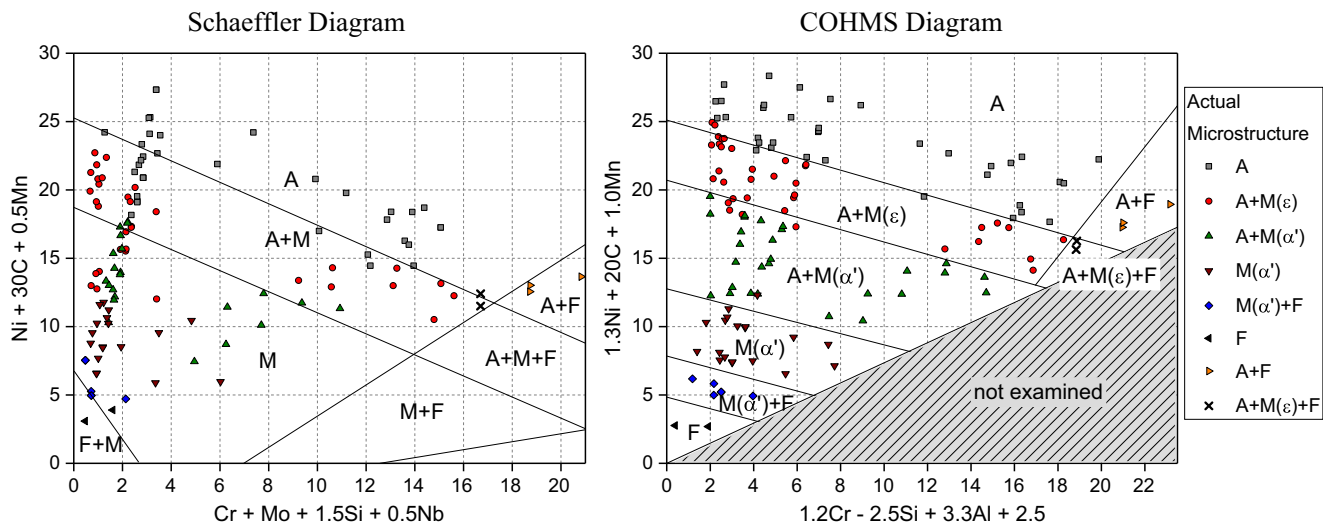
Fig. 8 Classification of the melting sample microstructures using the Schaeffler diagram (left) and the newly developed constitution diagram (right). Colors and symbols represent the type of microstructure present in the melting samples

resulting in cooling time $t_{8/5}$ between 9 and 22 s in the weld metal. Based on the metallographically determined dilution and the calculated chemical composition of the GMAW weld metals, the equivalents for the respective GMAW weld metals were determined and plotted in the COHMS diagram (see Fig. 9). The comparison of the actual and predicted weld metal microstructure shows that 89% of the GMAW weld metals are predicted correctly under the above welding conditions. The other 11% are in the near range of the boundary lines. Slight deviations in the area of the boundary lines cannot be avoided completely. On the one hand, the diagram was developed on the basis of a limited dataset and therefore represents a sufficiently accurate approximation solution for the underlying data. On the other hand, the formation of the weld metal

microstructure depends on many random influencing factors that cannot be fully taken into account. These include, for example, chemical inhomogeneities in base and filler metals, discontinuities in the welding process, varying cooling conditions, welding process-related burn-off, inaccuracies in the determination of the dilution, preparation-dependent micrographs, etc. Therefore, when applying the COHMS diagram in practice: The boundary lines are not to be considered as universal fixed boundaries between the different types of microstructure. As in the Schaeffler diagram and in all other constitution diagrams, the boundaries are to be understood as transitional areas determined under laboratory conditions. Especially between the regions A+M(ε) and A+M(α'), a transition area is to be assumed due to the possible concurrent

Fig. 9 Evaluation of the prediction accuracy of the COHMS diagram by recording the GMAW weld metals and comparing the predicted and actual microstructure. The actual type of microstructure corresponds to the colored symbols
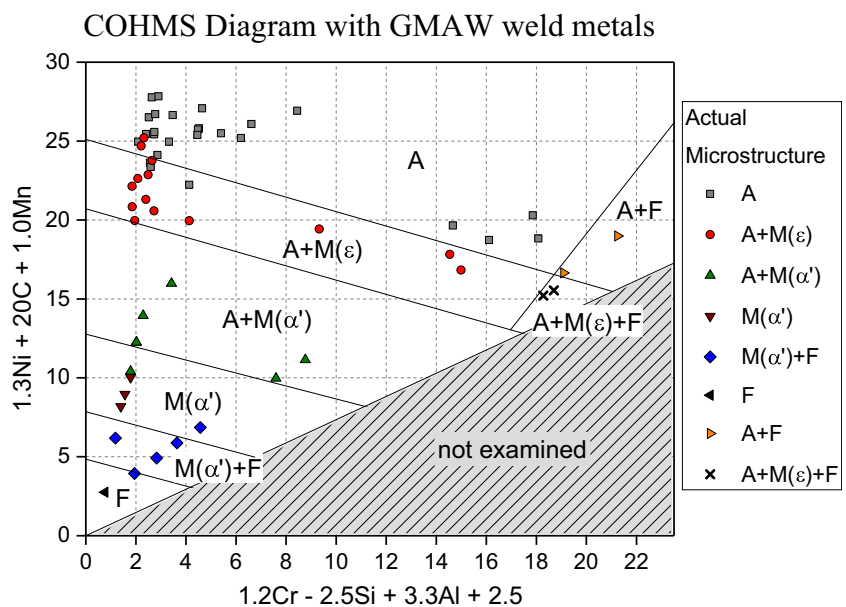
Table 2 Compositional range of confidence for the COHMS diagram

Elements [wt.-%]

C	Mn	Cr	Ni	Al	Si	Mo	Ti	N	(Mn+Ni)/Cr
0.06–0.66	0.9–19.1	0–19.3	0–8.5	0–2.3	0.09–2.23	0–0.35	0–0.02	0–0.3	> 0.78

presence of both types of martensite. In fact, the constitution diagrams are only valid under the test conditions under which they were established. This is why the COHMS diagram, as well as the other constitution diagrams, is a simple tool for predicting the resulting weld metal microstructure with sufficient accuracy.

3.4 Use and limits of the COHMS diagram

The new constitution diagram can be used in the same way as the Schaeffler diagram. The chemical composition of the base and filler metals are recorded as points in the diagram using the equivalent formulas and then connected by straight lines. With knowledge of the dilution, the point of the dissimilar weld metal can then be plotted on the connecting line and the microstructure expected at room temperature can be predicted.

The diagram was developed for dissimilar joints of austenitic Fe-Mn steels and low-alloyed ferritic or martensitic steels produced by GMAW welding. For this reason, the diagram may only be used for material combinations whose alloy contents are within the limits listed in Table 2. The compositional range of confidence is derived from the compositions of the used database. Moreover, the diagram is only adapted for conventional arc welding processes with cooling conditions comparable to those of a GMAW-CMT process (see above). Welding processes with high energy density, such as laser beam welding or resistance spot welding, result in very high heating and cooling rates as well as different mixing conditions. This may lead to differences in phase transformation behavior and weld metal microstructures. Furthermore, it is not recommended to extrapolate the microstructure regions outside the boundaries of the diagram.

3.5 Additional indication of weld metal hardness in the COHMS diagram

Based on the hardness values measured in the melting samples and GMAW weld metals, HV-ISO lines were determined and recorded in the COHMS diagram for additional estimation of the weld metal hardness (see Fig. 10). Above the < 300 HV line hardness values of less than 300 HV are to be expected. Hardness values between 300 and 350 HV can occur in the gray band below. Beneath this, a weld metal hardness of significantly greater than 350 HV is expected in the microstructure regions A+M(α'), M(α') and M(α')+F. The hardness only decreases again below 350 HV as soon as ferrite (F) in the weld metal is present.

4 Conclusions

1. An arc melting technique was used to experimentally simulate dissimilar weld metals. Thus the influence of the chemical composition on the resulting type of microstructure could be investigated effectively and a comprehensive dataset was generated.
2. It was shown that different types of martensite (ε and α') can form in dissimilar metal welds with Fe-Mn steels. Due to the very different properties, especially the hardness, they have to be distinguished.
3. By means of a discriminant analysis, a mathematical correlation between chemical composition and weld metal microstructure was developed. This enabled the derivation of new equivalent formulas. As a result, the COHMS diagram shows a significant better accuracy for microstructure prediction of high-manganese dissimilar metal welds than the Schaeffler diagram. It is also possible to distinguish and predict the different types of martensite (ε and α').
4. In addition to the microstructure prediction, the weld metal hardness can also be roughly estimated.
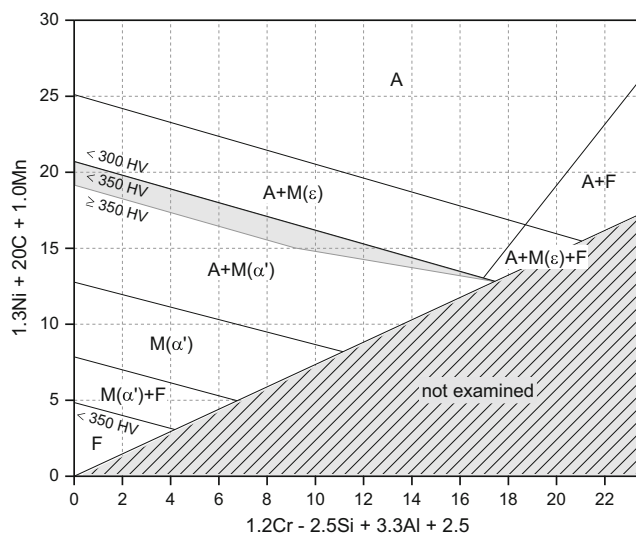

Fig. 10 COHMS diagram with additional HV-ISO lines to roughly estimate the resulting weld metal hardness

5. The new diagram should be applied only within the given compositional range of confidence and for conventional arc welding processes comparable to a GMAW-CMT process.

References

1. Otto, M. (2017) Fe-Mn-Al-Si-steels, lightweight potential for cars, trucks and trains. 5th International Conference on Steels in Cars and Trucks. Steel Institute VDEh, Düsseldorf

2. Kim, S. K.; Cho, J. W.; Kwak, W. J.; Kim, G.; Kwon, O. (2007) Development of TWIP steel for automotive application. 3rd international steel conference on new developments in metallurgical process technologies. Steel Institute VDEh, Düsseldorf

3. Keil D (2013) Beitrag zur Schweißeignung hoch manganhaltiger Stähle [Contribution to weldability of high manganese steels]. Otto von Guericke University Magdeburg, Dissertation

4. Graß, F.; Wesling, V.; Schram, A.; Flügge, W. (2016) Untersuchung zum Einfluss des Schweißzusatzes auf Mischverbindungen mit hochmanganhaltigen Stählen beim Laserstrahlschweißen [Investigation on the influence of the filler metal in dissimilar laser beam welds with high manganese steels]. DVS Berichte Band 327. Düsseldorf

5. Klueh RL, Maziasz PJ, Lee EH (1988) Manganese as an austenite stabilizer in Fe-Cr-Mn-C steels. Mater Sci Eng A 102:115–124. https://doi.org/10.1016/0025-5416(88)90539-3

6. Lee S, Lee C-Y, Lee Y-K (2015) Schaeffler diagram for high Mn steels. J Alloys Compd 628:46–49. https://doi.org/10.1016/j.jallcom.2014.12.134

7. Seyffarth, P. (1982) Atlas Schweiß-ZTU-Schaubilder [Atlas TTT welding diagrams]. Dt. Verl. für Schweisstechnik (DVS), Düsseldorf

8. DIN EN 10268 (2013) Cold rolled steel flat products with high yield strength for cold forming - technical delivery conditions

9. DIN EN 10083–3 (2007) Steels for quenching and tempering - part 3: technical delivery conditions for alloy steels

10. Balmforth MC, Lippold JC (1998) A preliminary ferritic-martensitic stainless steel constitution diagram. Welding Journal 77:1–7

11. Gould, E. K. (2010) Development of constitution diagram for dissimilar metal welds in nickel alloys and carbon and low-alloy steels. Master Thesis, The Ohio State University

12. Tordonato DS et al (2010) A new method for the design of welding consumables. Welding Journal 88:201–209

13. Balmforth, M. C.; Lippold, J. C. (2000) A new ferritic-martensitic stainless steel constitution diagram. Welding Journal, Welding Research Supplement 339–345

14. Wittig B, Zinke M, Jüttner S, Keil D (2017) Experimental simulation of dissimilar weld metal of high manganese steels by arc melting technique. Weld World 61:249–256. https://doi.org/10.1007/s40194-017-0427-z

15. Wittig, B.; Zinke, M.; Jüttner, S.; Seipp, A.; Schwabe, R. (2017) Procedure for developing a constitution diagram for dissimilar metal welds of high manganese steels. 5th international conference on steels in cars and trucks. Steel Institute VDEh, Düsseldorf.

16. Herold, H.; Wodara, J. (1994) Lexikon der Schweißtechnik [Welding Encyclopedia]. Dt. Verl. für Schweisstechnik (DVS), Düsseldorf

17. Schumann H (1966) Doppelte Martensitbildung in 13%igem Mn-Stahl [Double martensite formation in 13% Mn steel]. Neue Hütte 11:147–152

18. Schumann H (1972) Martensitische Umwandlungen in austenitischen Mangan-Kohlenstoff-Stählen [Martensitic transformations in austenitic manganese carbon steels]. Neue Hütte 17:605–609

19. Schlittgen R (2009) Multivariate Statistik [multivariate statistics]. Oldenbourg, München

20. Schumann H (1977) Austenitumwandlung in Stählen [Austenite transformation in steels]. Neue Hütte 22:296–301

21. Wittig, B.; Zinke, M.; Jüttner, S. (2018) Gefüge- und Eigenschaftsvorhersage für das Schweißen hochmanganhaltiger Stähle in Mischverbindung [Prediction of dissimilar weld metal microstructure and properties of high manganese steels]. Research Report. (AiF Research Project IGF-No. 18.660 BR). Institute of Materials and Joining Technology, Otto von Guericke University Magdeburg

22. Zhao C (2000) Relationships between martensite transformation temperatures and compositions in Fe-Mn-Si-based shape memory alloys. Proceedings of the Institution of Mechanical Engineers, Part L: Journal of Materials: Design and Applications 214:173–176. https://doi.org/10.1177/146442070021400306